PCCP

Accepted Manuscript

ROYAL SOCIETY OF CHEMISTRY

www.rsc.org/pccp

Adsorption of Fluoride from Aqueous Solutions onto Fe-Impregnated Chitosan and mechamism study

Jing Zhang[a], Nan Chen[a,*], Zheng Tang[b], Yang Yu[a], Qili Hu[a] and Chuanping Feng[a,*]

[a]School of Water Resources and Environment, China University of Geosciences (Beijing), Beijing 100083, China

[b]Beijing Synchrotron Radiation Facility, Institute of High Energy Physics, Chinese Academy of Sciences, Beijing 100049, China

ABSTRACT: The adsorption of fluoride from aqueous solutions onto an Fe-impregnated chitosan (Fe-CTS) granular adsorbent was studied, and the adsorption capacity was determined to be 1.9736 mg/g at an initial fluoride concentration of 10 mg/L. The effects of the initial fluoride concentration, dosage, and temperature were investigated using factorial design and analysis. The results indicated that high initial fluoride concentrations, low dosages, and low temperatures could enhance the fluoride adsorption capacity. In addition, Fe-CTS exhibited high selectivity for fluoride removal in the presence of high levels of several coexisting anions (nitrate, chloride, bicarbonate, and phosphate), except carbonate and sulfate. The adsorption process followed the Langmuir model at low fluoride concentrations and the Freundlich model at high initial fluoride concentrations. The data also fit the pseudo-second-order model. Scanning electron microscopy (SEM), Fourier-transform infrared (FTIR) spectroscopy, and extended X-ray absorption fine-structure (EXAFS) spectroscopy were used to elucidate the adsorption mechanism. The FTIR and EXAFS analyses revealed that Fe was chelated with $–NH_2$ and –OH groups on the CTS, and fluoride adsorption on the Fe-CTS occurred due to ion exchange between chloride and fluoride.

Keywords: Fe-impregnated chitosan; Fluoride adsorption; Ion exchange; Coexisting anions

Highlights

●A granular Fe-impregnated chitosan (Fe-CTS) adsorbent was synthesized by chelating Fe ions to –OH and $–NH_2$ groups of CTS.

●The Fe-CTS granular adsorbent exhibited high performance for the adsorption of fluoride.

●The mechanism of fluoride adsorption on Fe-CTS was elucidated using EXAFS and FTIR analyses.

● Fluoride adsorption on Fe-CTS occurred via ion exchange between chloride and fluoride.

1. Introduction

The presence of fluoride in drinking water can have beneficial or detrimental effects on human health depending on its concentration [1]. Fluoride is an essential component of the human body and is involved in the formation of caries-resistant dental enamel and the normal mineralization process in hard tissues at low concentrations of approximately 0.7 mg/L [2,3]. However, excessive dosages can lead to toxic and chronic effects; the maximum dosage recommended by the World Health Organization (WHO) is 1.5 mg/L [4]. It is estimated that high fluoride concentrations are present in groundwater in at least 25 countries, particularly in parts of South America, central Africa, China, and India [5]. Reducing fluoride concentrations is therefore necessary to provide safe drinking water.

Various techniques have been developed to efficiently remove fluoride ions from water such as coagulation [6], ion exchange [7], electrocoagulation [8], nanofiltration [9], catalytic ozonation [10], electrochemical oxidation [11], and adsorption [12]. Adsorption techniques have attracted attention in recent decades because they are simple, cheap, rapid, and highly efficient. Numerous studies have

focused on the application of natural materials, including chitosan (CTS) [13], *Citrus limonum* (lemon) leaves [14], carbonaceous materials produced from coffee grounds [15], lateritic soils [16], bone char [17], and Kanuma mud [18], for defluoridation of aqueous solutions. It has also been reported that the impregnation of metal compounds such as Zr(IV) on cellulose [19] and a polystyrene anion exchanger [20], La(III) on a granular ceramic [21], and Al(III) on scoria [22] increases their fluoride adsorption capacities.

In addition, many researchers have modified chitosan with single or binary metals for defluoridation because unmodified CTS runs off easily and has a low fluoride adsorption capacity. Tang et al. [23] reported that the adsorption capacity of fluoride after a contact time of 48 h increased from 0.052 mg/g on pure chitosan to 0.69 mg/g on chitosan-coated alumina (CAL). Thakre et al. [24] used a Ti–Al binary metal oxide to modify chitosan, and the adsorption capacity for this material reached approximately 1.10 mg/g with a contact time of 24 h. However, the contact times for these adsorbents were relatively long and their adsorption capacities were low. Furthermore, the adsorption mechanisms of modified chitosan had not yet been revealed clearly.

Therefore, to further enhance the fluoride adsorption capacity of chitosan, in the present study, an Fe-impregnated CTS (Fe-CTS) granular adsorbent was prepared by impregnating a commercially available CTS with ferric chloride. The effects of the initial fluoride concentration, dosage, and temperature on fluoride adsorption were investigated using factorial design and analysis. In addition, the selectivity for fluoride in the presence of other ions was investigated over a wide range of coexisting ion concentrations. The adsorption behavior of the adsorbent was also evaluated using adsorption kinetics and isotherm studies. Furthermore, scanning electron microscopy (SEM) and Fourier-transform infrared (FTIR) and extended X-ray absorption fine-structure (EXAFS) spectroscopy were used to elucidate the mechanism of fluoride adsorption on the Fe-CTS.

2. Materials and methods

2.1 Chemicals

NaF was purchased from National Medicines (Shanghai, China), and a fluoride stock solution (100 mg/L) was prepared by adding NaF (0.2210 g), which was dried at 105 °C for 2 h, to deionized water (1000 mL). The test solutions were prepared via subsequent dilution of the stock solution. CTS with a deacetylation degree of 80.0–95.0% was purchased from National Medicines (Shanghai, China). The reagents $NaHCO_3$, Na_2CO_3, $NaNO_3$, Na_3PO_4, NaCl, and Na_2SO_4 were purchased from National Medicines (Shanghai, China). All chemicals used in this study were of analytical reagent grade.

2.2 Synthesis of the Fe-CTS granular adsorbent

CTS (1.25 g) was dissolved in a 2% acetic acid solution (50 mL), and the mixture was stirred at room temperature for 0.5 h. Subsequently, $FeCl_3 \cdot 6H_2O$ (5.0 g) was added, and the resultant mixture was continuously stirred for 0.5 h. After standing for a further 0.5 h, the prepared mixture was dropped into a 6.25% ammonia solution, after which gel beads were formed. The beads were dried at 50 °C for 12 h and then reacted with ammonia solution for 1 h to afford the Fe-CTS granular adsorbent (Fe-CTS).

2.3 Batch adsorption experiments

To investigate the ability of the Fe-CTS adsorbent to remove fluoride from aqueous solutions, batch experiments were conducted by reacting different fluoride solutions (50 mL) in 200 mL conical flasks with the adsorbent (0.25 g). The conical flasks were placed in a shaker and shaken at 150 rpm and 30°C

for 6 h. The aqueous samples were then filtered through a 0.45 μm cellulose acetate filter.

The adsorption kinetic studies were conducted by varying the initial fluoride concentration (5, 10, and 15 mg/L) at 30°C. Adsorption isotherm studies were performed at initial fluoride concentrations of 5, 10, 15, 25, 50, 75, and 100 mg/L at 25, 30, 40, 50, and 60°C. The effects of coexisting anions (HCO_3^-, CO_3^{2-}, NO_3^-, PO_4^{3-}, Cl^-, and SO_4^{2-}) were investigated at an initial fluoride concentration of 10 mg/L.

The amount of fluoride adsorbed per unit weight of Fe-CTS granular adsorbent, q_e (mg/g), was calculated using the following equation [25]:

$$q_e = \frac{(C_0 - C_e)\cdot V}{m} \quad (1)$$

where C_0 and C_e are the initial and equilibrium fluoride concentrations (mg/L), respectively, V is the volume of the aqueous solution (L), and m is the mass of the adsorbent used (g).

2.4 Factorial design

The effects of various factors on fluoride adsorption by the Fe-CTS adsorbent were investigated using a 2^3 factorial design. As shown in Table 1, three factors, i.e., the initial fluoride concentration, adsorbent dosage, and temperature at two levels were varied.

The main effect of each factor was determined using the following expression [26]:

$$A = (a-1)(b+1)(c+1)/4 \quad (2)$$

The interactions among the factors were described as follows [27]:

$$AB = (a-1)(b-1)(c+1)/4 \quad (3)$$

$$ABC = (a-1)(b-1)(c-1)/4 \quad (4)$$

where a, b, and c represent high levels for the three factors, and 1 represents low levels for the factors. It is worth noting that these expressions must be opened up when used; for example, in the expanded form, a represents the adsorption capacity of the sample at a high level of a, low level of b, and low level of c, while abc represents high levels of a, b, and c.

Table 1. High and low level factors used in 2^3 factorial design

Factors	Low level	High level
A	10	100
B	0.2	5
C	30	60

A: initial concentration (mg/L); B: dosage (g/L); C: temperature (°C)

2.5 Error analysis

The quality of the fitting of the experimental data to the adsorption kinetics and isotherm models was evaluated using error function assessments, i.e., the residual root-mean-square errors (RMSE), absolute errors (SAE), and $\varkappa^2$ tests. The values RMSE, SAE, and $\varkappa^2$ are given by Eqs.(5), (6), and (7), respectively [28,29].

$$RMSE = \sqrt{\frac{1}{n-p}\sum_{i=1}^{n}(q_{e,\exp} - q_{e,cal})_i^2} \quad (5)$$

$$SAE = \sum_{i=1}^{n} \left| q_{t,\exp} - q_{t,cal} \right|_i \quad (6)$$

$$\chi^2 = \sum_{i=1}^{n} \left[\frac{(q_{e,\exp} - q_{e,cal})^2}{q_{e,cal}} \right] \quad (7)$$

where $q_{e,exp}$ and $q_{e,cal}$ are the experimental and calculated equilibrium adsorption capacities, respectively; $q_{t,exp}$ and $q_{t,cal}$ are the experimental and calculated adsorption capacities at time t, respectively; n is the number of experimental data points; and p is the number of parameters in the model equation. The experimental data obeyed one model well when the RMSE, SAE, and $\varkappa^2$ values were close to zero.

2.6 Analytical methods

The fluoride concentration was determined using a UV spectrophotometer (DR6000, HACH, USA) [30]. Surface morphological analysis was performed using SEM (SSX-550, Shimadzu, Japan). FTIR spectra were recorded (Nexus 470, Nicolet, USA) using KBr pellets over the wavenumber range 4000–400 cm^{-1}. Raman spectra were obtained using a laser (λ = 473 nm, P = 100 mW) in the backscattering configuration (LabRAM HR Evolution, Horiba, France). EXAFS experiments were conducted at the XAFS station (1W2B beamline) of the Beijing Synchrotron Radiation Facility. Adsorbent samples were ground to fine powders and then smeared on Scotch tape or pressed into thin slices. Fe K-edge EXAFS spectra were collected at room temperature in transmission mode. The storage ring was operated at 2.5 GeV with a maximum electron current of approximately 250 mA.

3 Results and discussion

3.1 Fe-CTS characterization

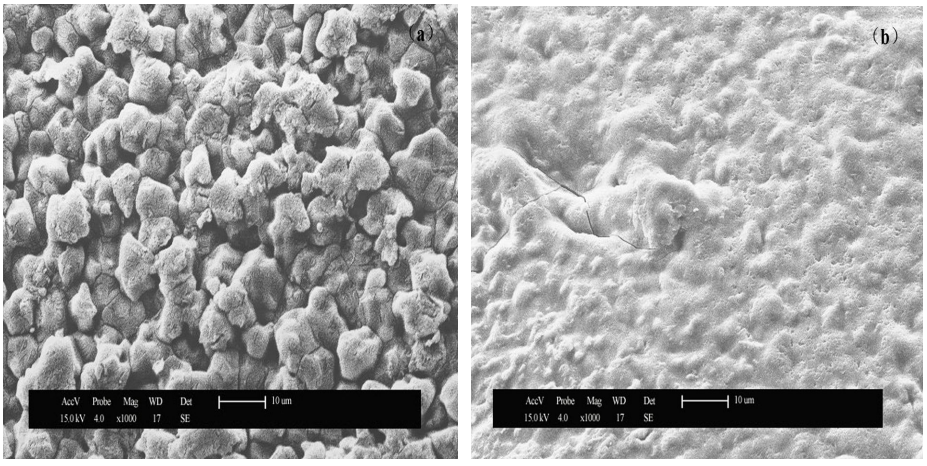

Fig. 1. SEM images of Fe-CTS
(a): before adsorption; (b): after adsorption for 6 h.

The Fe-CTS granular adsorbent consisted of hard black spherical particles with diameters of 1.5–2.0 mm. SEM images (1000×) of the adsorbents before and after fluoride adsorption (Fig. 1a and b) revealed important differences in the surface morphology after fluoride adsorption. The Fe salt initially formed an uneven surface structure on the CTS (Fig. 1a), similar to that observed for a magnetic chitosan-Fe(III) hydrogel [31]. These surface irregularities are often formed when polymer particles

loaded with an insoluble material are prepared via suspension of the polymer in an aqueous solution [32]. However, they were different from those reported for Fe(III)-loaded carboxylated chitosan beads (Fe-CCB) [33], with a greater number of irregularities observed on the surface of the Fe-CTS resulting in a higher adsorption capacity. This difference may be due to the use of chloroacetic acid for the synthesis of Fe-CCB, which may have reacted with the -OH groups on the chitosan, leading to a reduction in the number of binding sites for Fe(III). Furthermore, after fluoride adsorption, the surface of the Fe-CTS was smooth and had no sharp edges, which may be attributed to the complexation of F ions by Fe followed by precipitation of Fe-F complexes on the surface of the Fe-CTS. Consequently, the surface morphology changed. It should also be noted that the difference in the Fe-CCB and Fe-CTS surfaces after adsorption implied that different adsorption mechanisms were involved for the two adsorbents. While both formed complexes with fluoride ions, they likely had different structures, which resulted in different surface morphologies.

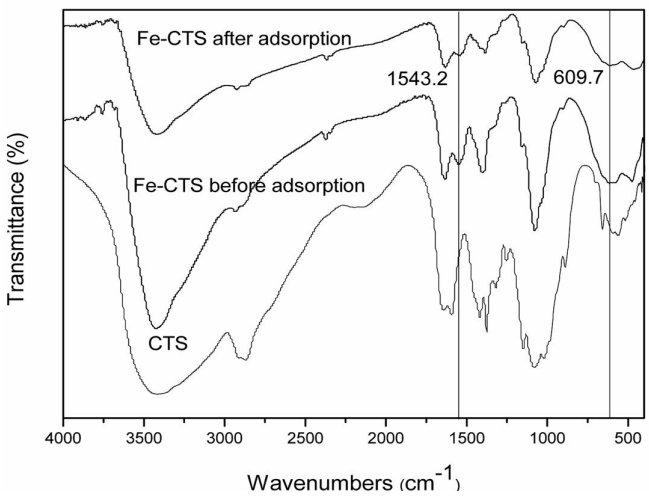

Fig. 2. FTIR spectra of CTS and Fe-CTS before and after fluoride adsorption.

FTIR spectra of CTS and Fe-CTS before and after fluoride adsorption are shown in Fig. 2. The broad band at 3450 cm^{-1} associated with the stretching vibrations of H_2O molecules [34], the axial stretching vibration of O-H superimposed on the N-H stretching band, and intermolecular hydrogen bonds of the polysaccharide in the spectrum of Fe-CTS indicated that coordination of the Fe to CTS occurred via free hydroxyl and amido groups in the CTS [35]. In addition, the peak centered at 2927 cm^{-1} was assigned to CTS C-H vibrations [36], while the characteristic absorption bands at 1628, 1543, and 1396 cm^{-1} represented N-H deformation, amido H-N-H deformation, and C-N stretching vibrations [37], respectively. The newly emerged H-N-H deformation band in the Fe-CTS spectrum before fluoride adsorption indicated Fe chelation of $-NH_2$ groups in the CTS. Furthermore, the disappearance of the O-H deformation band centered at 1259 cm^{-1} in the spectrum of Fe-CTS indicated that the Fe was also chelated with -OH groups of the CTS. Hernandez et al. [38] reported similar results for the coordination of chitosan and Fe^{3+}. The sharp peak at 1070 cm^{-1} and the broad band at 500–800 cm^{-1} were related to the C-O [39] and metal–oxygen (Fe-O) bonds in the coordinated complexes [40], respectively. The appearance of the Fe-O band in the spectra for Fe-CTS before and after fluoride adsorption indicated that the $FeCl_3$ was complexed by the CTS. The fact that no significant changes were observed in the Fe-CTS spectra before and after fluoride adsorption revealed that no significant structural changes occurred in the adsorbent during the adsorption process.

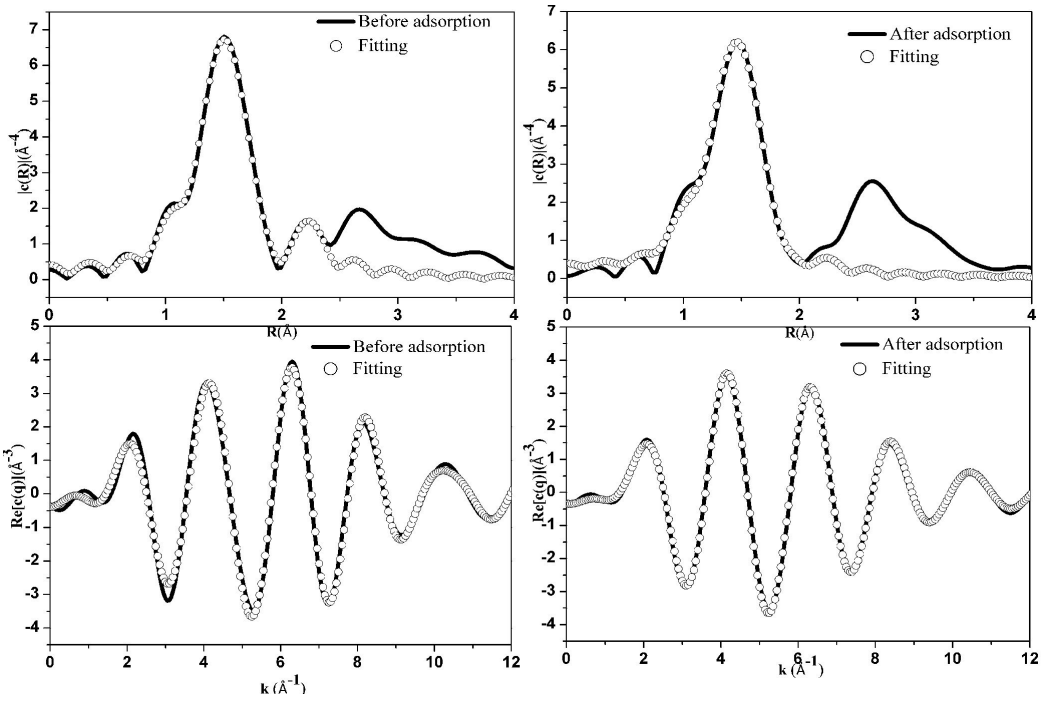

Fig. 3. Least-squares fitting results in R and q spaces for samples before and after adsorption.

Fig. 3 shows the fitting results in the R and q spaces. EXAFS analysis of the Fe K-edge using the Athena [41] and Artemis [42] programs was performed to investigate the microscopic adsorption mechanism. Background removal, normalization, Fourier transform, and backward Fourier transform were performed using the Athena program. The Fourier-transform analysis was conducted in the k range from 2.5 to 12 $Å^{-1}$ using a Hanning window and weighting the EXAFS oscillation with k^3, and the backward Fourier transform analysis was conducted in the R ranges from 1 to 2.4 Å and 1 to 2 Å for samples before and after adsorption, respectively. Least-squares fitting was performed using the Artemis program. For the un-adsorbed sample, the first coordination shell was divided into two subshells, namely Fe–O and Fe–N, and the second coordination shell was Fe–Cl. The theoretical scattering paths employed for the fitting were generated using the FEFF 6.0 calculation code based on a modified goethite Fe(OOH) structure [43] (by replacing one of the oxygen atoms with a nitrogen atom) and $FeCl_3$. For the sample with adsorbed fluoride ions, the first coordination shell was divided into three subshells, i.e., Fe–O, Fe–N, and Fe–F. The two theoretical scattering paths for Fe–O and Fe–N were the same as those for the sample with no adsorbed fluoride, and the scattering path for Fe–F was based on FeF_3. During the fitting, only single scattering paths were considered, and an amplitude reduction factor (S_0^2) of 0.70 was obtained from the fitting of the EXAFS spectrum for a reference Fe foil.

The coordination numbers (N), bond distances (R), and Debye–Waller factors are listed in Table 2. It can be seen from Table 2 that the coordination numbers and bond distances in the Fe–O and Fe–N subshells remained nearly unchanged during the adsorption process. However, the bond distance between the adsorbent molecules decreased from 2.66±0.03 Å to 2.12±0.02 Å after adsorption, indicating that the second-shell Fe–Cl disappeared and an Fe–F subshell appeared. This result revealed that the microscopic adsorption mechanism was ion exchange between F and Cl ions. The adsorbent R factors were both near zero before and after adsorption (0.0002 and 0.0001, respectively) indicating

that the calculated data were in good agreement with the experiment results.

Table 2. Fe K-edge EXAFS structure parameters of samples before and after adsorption

Sample	Path	R (Å)	*n*	σ^2 (Å^2)	R factor
Before adsorption	Fe-O	1.94±0.02	2.11±0.4	0.003±0.001	0.0002
	Fe-N	2.10±0.02	1.96±0.5	0.003±0.001	
	Fe-Cl	2.66±0.03	0.61±0.4	0.007±0.002	
After adsorption	Fe-O	1.93±0.02	2.15±0.5	0.003±0.002	0.0001
	Fe-N	2.08±0.02	1.94±0.4	0.003±0.002	
	Fe-F	2.12±0.02	0.58±0.4	0.003±0.002	

To further verify the occurrence of ion exchange between F and Cl ions, the Raman spectra of the Fe-CTS adsorbent before and after fluoride adsorption were obtained (Fig. 4). The peaks at 225 and 280 cm^{-1} were attributed to Fe-Fe vibrations, and the increase in intensity for both peaks after adsorption was due to the enhanced A_{1g} complexation mode [44]. The peaks centered at 375 and 580 cm^{-1} were assigned to Fe-Cl and Fe-N [45] vibrations, respectively. The appearance of two new peaks after adsorption at 485 and 533.5 cm^{-1} associated with Fe-F vibrations [46] indicated that complexation between Fe and F ions occurred. However, observation of any notable change in the intensity of the Fe-Cl peak was difficult possibly because only a small amount of Cl and F ions were exchanged in the 10 mg/L fluoride solution. Thus, to investigate the relationship between the fluoride and chloride ions, changes in the F^- and Cl^- molar concentrations after adsorption using aqueous solutions containing different initial fluoride concentrations were determined. The results indicated that the Cl^- molar concentration increased as the quantity of fluoride adsorbed on the Fe-CTS increased, and the ratio of the changes in the F^- and Cl^- molar concentration followed the same tendency, with the change in fluoride concentration slightly higher than that of the chloride. This behavior confirmed the occurrence of ion exchange between the F and Cl ions.

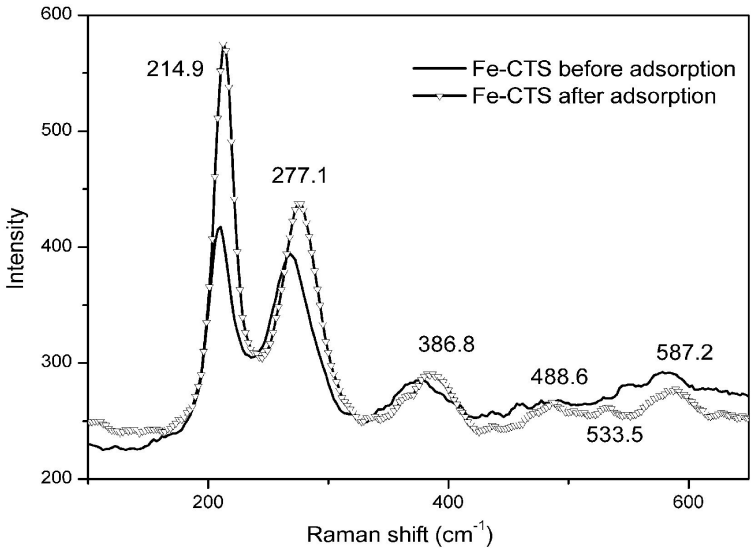

Fig. 4. Raman Spectra of Fe-CTS before and after fluoride adsorption.

3.2 Adsorption kinetics

Pseudo-first-order and pseudo-second-order kinetic models [33] were used to fit the experimental data for fluoride adsorption to determine the adsorption mechanism and potential rate-controlling steps.

$$\log(q_e - q_t) = \frac{\log q_e - k_1 t}{2.303} \tag{8}$$

$$\frac{t}{q_t} = \frac{1}{k_2 q_e^2} + \frac{t}{q_e} \tag{9}$$

where q_t and q_e are the quantities of fluoride adsorbed at time t and at equilibrium (mg/g), respectively, and k_1 and k_2 are the first-order and second-order rate constants, respectively, for fluoride adsorption. The adsorption kinetic parameters obtained for these two models are shown in Table 3. Higher correlation coefficient values (R^2 = 0.9950, 0.9957, and 0.9945) and smaller RMSEs (0.0439, 0.0830, and 0.1504) and SAEs (0.2842, 0.5268, and 0.8632) were obtained for the pseudo-second-order kinetic model compared to those obtained for the pseudo-first-order kinetic model (R^2 = 0.9246, 0.9695, and 0.9644; RMSE = 0.1554, 0.1114, and 0.1225; SAE = 2.4346, 3.8582, and 4.0538), indicating that fluoride adsorption on the Fe-CTS granular adsorbent fitted the pseudo-second-order kinetic model at initial fluoride concentrations ranging from 5 to 15 mg/L. Smaller SAE and RMSE values indicated smaller differences between the calculated q_t and experimental q_t values. In addition, the adsorption rate constant K_2 decreased with the initial concentration, suggesting that chemisorption was the rate-controlling step in the fluoride adsorption process and the rate of fluoride adsorption depended on the availability of adsorption sites rather than the adsorbate concentration in solution [47,48]. Viswanathan et al. [33], Shen et al. [31], and Zhu et al. [35] also reported that the adsorption of fluoride on chitosan-based adsorbents follows pseudo-second-order kinetics, indicating that chemisorption is the rate-controlling step in the adsorption process.

Table 3. Kinetic parameters of different initial concentration with error analysis for fluoride adsorption on Fe-CTS

Model	Parameters	Fluoride initial concentration

		5 mg/L	10 mg/L	15 mg/L
	q_e (mg/g)	0.6291	1.4228	2.3152
	K_1 (min^{-1})	0.0170	0.0196	0.0199
Pseudo-first-order	R^2	0.9246	0.9695	0.9644
	SAE	2.4346	3.8582	4.0538
	RMSE	0.1554	0.1114	0.1225
	q_e (mg/g)	1.0449	2.1420	3.1623
	K_2 (mg/(g·min))	0.0376	0.0177	0.0108
Pseudo-second-order	R^2	0.9950	0.9957	0.9945
	SAE	0.2842	0.5268	0.8632
	RMSE	0.0439	0.0830	0.1504

3.3 Adsorption isotherm studies

The data obtained from the experiments were fitted to three commonly used isotherm models (Langmuir, Freundlich, and Redlich–Peterson), and the adsorption isotherm parameters and equations are listed in Table 4. High correlation coefficients were obtained using the Langmuir (R^2 = 0.9988 at 25°C, 0.9996 at 30°C, 0.9992 at 40°C, 0.9946 at 50°C, and 0.9988 at 60°C) and Redlich–Peterson (R^2 = 0.9988 at 25°C, 0.9997 at 30°C, 0.9991 at 40°C, 0.9939 at 50°C, 0.9219 at 60°C) models with a small $\varkappa^2$. Specifically, the experimental data fitted the Langmuir isotherm model well when the initial fluoride concentration was 10 mg/L. The Redlich–Peterson isotherm model gave somewhat higher R^2 coefficient and lower $\varkappa^2$ and RMSE values at lower temperatures (25, 30, 40, and 50°C), while the Langmuir isotherm model gave higher R^2 coefficient and lower $\varkappa^2$ and RMSE values at 60 °C. Therefore, at 25, 30, 40, and 50 °C, fluoride adsorption onto Fe-CTS followed a Langmuir model at an initial fluoride concentration of 5 mg/L, but followed the Freundlich model at an initial fluoride concentration of 100 mg/L. Consequently, at low initial fluoride concentrations, the adsorption process involved monolayer adsorption with equal enthalpies and energies for all sites, whereas at high initial fluoride concentrations, adsorption occurred on heterogeneous surfaces probably in a multilayer form [49]. In addition, at 60 °C, the adsorption process followed the Langmuir isotherm well at both low and high fluoride initial concentrations. The dimensionless constants R_L were between 0 and 1, and the values for $1/n$ were less than 1, indicating that adsorption was favored [50]. Moreover, the R_L constants increased as the temperature increased, indicating that low temperatures promoted fluoride adsorption, which was in good agreement with the decrease in the Q_0 values as the temperature increased. Finally, for the Freundlich model, the value for n obtained at 60°C was less than the values for n at 25, 30, 40, and 50°C, suggesting that high temperatures inhibited multilayer adsorption.

Table 4. Isotherm parameters of different temperatures with error analysis for fluoride adsorption on Fe-CTS

Isotherm model	Linear form	25°C	30°C	40°C	50°C	60°C
Langmuir	$C_e/q_e = 1/(bQ_0)+C_e/Q_0$					
Q_0 (mg/g)		20.4040	20.7464	19.5409	18.3670	19.8661
b (L/mg)		0.0992	0.0832	0.0855	0.0833	0.0530
R_L		0.5019	0.5459	0.5390	0.5456	0.6535
R^2		0.9988	0.9996	0.9992	0.9946	0.9988
$\varkappa^2$		0.0305	0.02726	0.0196	0.1527	0.0854

RMSE		0.9047	0.9644	0.8428	0.8428	1.0024
Freundlich	$\ln q_e=\ln K_f+1/n\cdot\ln C_e$					
n		1.8220	1.7280	1.8135	1.7795	1.5880
K_f(mg/g)		2.5646	2.4077	2.2627	2.2465	1.7719
R^2		0.9740	0.9715	0.9749	0.9656	0.9709
$\varkappa^2$		0.8185	0.9301	0.7103	1.0047	0.8438
RMSE		0.9047	0.9644	0.8428	1.0024	0.9186
Redlich-peterson	$\ln(K_R C_e/q_e-1)=\beta\ln C_e+\ln a_R$					
K_R		2.0591	1.7077	1.6883	1.6147	0.0151
a_R		0.1028	0.0483	0.0849	0.0592	-0.9923
β		0.9920	1.1292	1.0018	1.0830	-0.0063
R^2		0.9988	0.9997	0.9991	0.9939	0.9219
$\varkappa^2$		0.0379	0.0095	0.0245	0.1789	2.2688
RMSE		0.1742	0.0873	0.1401	0.3783	1.3472

3.4 Factorial analysis

The main effects of the three factors and their interactions on fluoride adsorption by the Fe-CTS adsorbent are displayed in Table 5. Interactions between the initial concentration, dosage, and temperature and between the temperature and dosage were very close to zero and small enough to be neglected. On the other hand, both initial fluoride concentration and dosage had large effects on fluoride adsorption as reflected by their main effect values of 21.47 and −27.43, respectively. The initial fluoride concentration had a positive effect, whereas the dosage had a negative effect on the adsorption process [51]. The main effect values for the temperature and its interaction with the initial concentration were 0.61 and −2.27 respectively, indicating that both had little effect on the adsorption capacity. Further, analysis of the F distributions revealed that the value for $F_{0.05}(1, 2)$ of 18.5. Notably, the F values for both A (91.51) and B (152.25) were greater than 18.5, indicating that the effects of the adsorbent dosage and initial fluoride concentration on fluoride adsorption were greater than that of temperature (1.65) [52]. To increase the fluoride adsorption capacity, therefore, adsorption should be performed at a high initial fluoride concentration, low dosage, and low temperature.

Table 5. Estimated effects and Seq-SS values for removal efficiency

Factors	Main effect or their interactions	DF	Seq-SS	F-value
A	21.47	1	1808.69	91.51
B	-27.43	1	3009.15	152.25
C	0.61	1	32.64	1.65
AB	-8.08	1	261.27	13.22
AC	-2.27	1	20.65	1.04
MSE		2	19.77	

3.5 Effects of coexisting anions

Sulfate, nitrate, bicarbonate, carbonate, chloride, and phosphate ions are typically present in fluoride-contaminated water and compete with fluoride for active adsorption sites, thus, decreasing the removal efficiency of the adsorbent [53]. As shown in Fig. 5, the presence of these anions at concentrations ranging from 5 to 200 mg/L had little effect on the fluoride removal efficiency. The presence of chloride and bicarbonate slightly increased the fluoride removal capacity by 0.58 mg/g at 100 mg Cl^-/L and 2.53 mg/g at 5 mg HCO_3^-/L, respectively. However, the removal efficiency decreased significantly from 87.99% to 69.22% and from 86.59% to 43.35%, respectively, when the concentrations of carbonate and sulfate increased from 0 to 200 mg/L. The order of the effect of the ions was $HCO_3^- > Cl^- > NO_3^- > PO_4^{3-} > SO_4^{2-} > CO_3^{2-}$, which is similar to those previously reported for fluoride adsorption on lanthanum-impregnated chitosan (La-chitosan) [54] and chitosan-based mesoporous Ti–Al binary metal oxide-supported beads [21], except for HCO_3^-. In these previous studies, HCO_3^- had the largest effect on adsorption, while in the present study HCO_3^- had the smallest effect on adsorption (other than Cl^- and NO_3^-, which had positive effects on fluoride adsorption). It is possible that bicarbonate reacted with the ammonium acetate formed in the Fe-CTS synthesis process and was partially converted to carbon dioxide, ammonia, and acetate in the acidic solution (pH 5.23), leading to a decrease in the ammonium acetate concentration. Such a scenario could also explain why the effect of the bicarbonate was greater at higher bicarbonate concentrations. It should also be noted that the decrease in the removal efficiency via fluoride adsorption onto Fe-CTS due to the presence of bicarbonate ions was less than that observed for the La-chitosan [54] and binary metal oxide supported beads [24]. Moreover, multivalent anions had negative effects possibly because they were involved in stronger electrostatic interactions with the positively charged adsorbents [24].

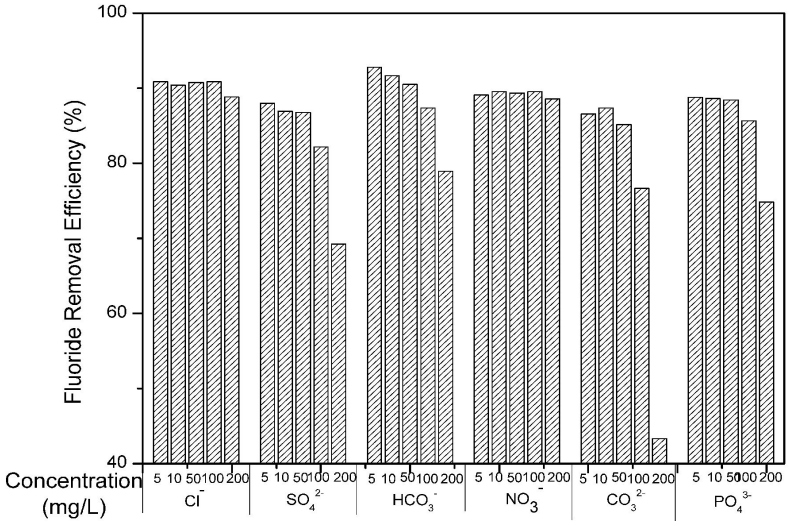

Fig. 5 Effect of coexisting anions on fluoride removal.

3.6 Adsorption mechanism

Spectroscopic analysis provided valuable information on the fluoride adsorption process using Fe-CTS. Specifically, the main functional groups involved in anchoring the Fe(III) ions on CTS and in the adsorption of fluoride were identified. These analyses also helped to identify the ferric fluoride species on the adsorbent surface.

The experimental kinetic studies revealed that the process was rapid, and an adsorption removal efficiency of approximately 80% was achieved within 1 h. It was also demonstrated that the adsorption

rate depended on the number of available adsorption sites on the adsorbent surface, and was eventually controlled by the binding of fluoride to the surface [29,55]. Compared to a maximum adsorption capacity of 0.052 mg/g on raw CTS [33], an adsorption capacity of 1.9736 mg/g was obtained in the present study with Fe-CTS. Furthermore, the adsorption capacity of Fe-CTS was higher than that of CAL (0.69 mg/g) [23] and the Ti–Al binary metal oxide supported chitosan beads (1.10 mg/g) [24], indicating that the number of available adsorption sites increased when the CTS was chelated with the Fe ions [38].

On the basis of the results obtained in the present study, possible mechanisms for the synthesis of Fe-CTS and fluoride adsorption on the adsorbent were postulated, which are shown in Fig. 6. The Fe ions in CTS are hexacoordinated, with at least one water molecule in the coordination sphere of the metal ion [56]. Therefore, chelation between Fe ions and CTS was assumed to occur, as shown in Fig. 6 (a). The Fe ions were chelated by two –OH, two $–NH_2$ groups on CTS, one water molecule, and one chlorine atom.

Fluoride adsorption on the Fe-CTS is shown in Fig. 6 (b). Analysis of the EXAFS spectra revealed that the highest peak was displaced, indicating that shorter Fe–F bond formed instead of the original Fe–Cl bonds. However, no further changes in the structure of the Fe-CTS after adsorption were observed, indicating that the mechanism of fluoride adsorption by Fe-CTS was an ion exchange process, i.e., fluorine replaced chlorine and then formed the Fe–F bond because fluorine and chlorine are congeners and have similar chemical properties. In contrast, fluoride adsorption on Fe-CCB occurs via electrostatic adsorption followed by the reaction of Fe and F ions to form complexes [33]. The differences in the adsorption processes on Fe-CTS and Fe-CCB resulted in different structures for the two Fe-complexed adsorbents, as was observed by SEM (Fig. 1).

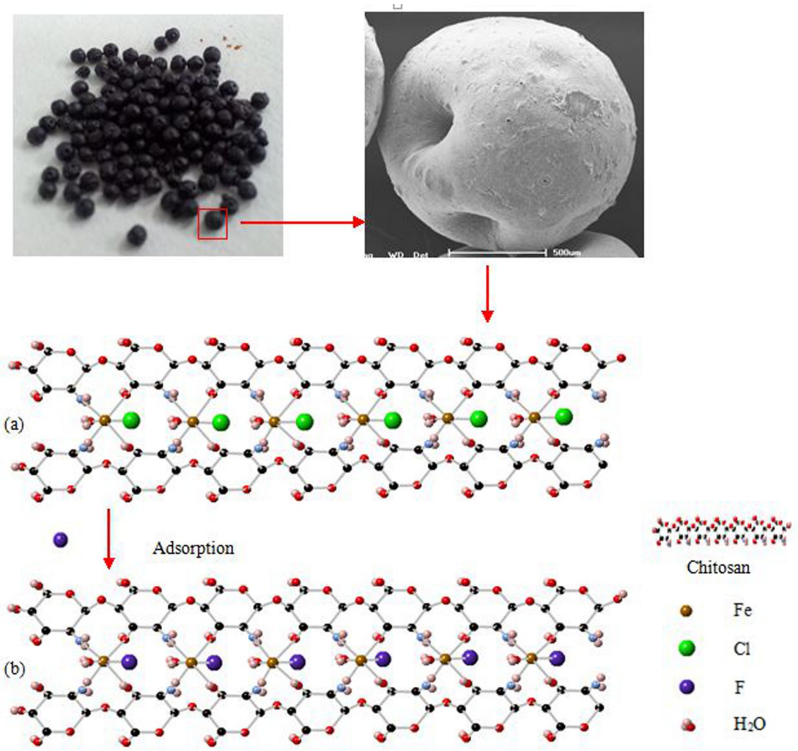

Fig. 6. Proposed chelation of Fe^{3+} with CTS, and fluoride adsorption mechanism.
(a): Fe-CTS before adsorption, (b): Fe-CTS after adsorption

4. Conclusion

A synthesized Fe-CTS granular adsorbent exhibited good adsorption capability for fluoride removal. Factorial analysis revealed that the fluoride adsorption capacity increased at higher initial fluoride concentrations, low dosages, and low temperatures. Coexisting anions, except carbonate and sulfate at high concentrations, did not inhibit fluoride removal, demonstrating that Fe-CTS had high selectivity for fluoride. The adsorption isotherms were described well by the Langmuir model at low initial fluoride concentrations and by the Freundlich model at high initial fluoride concentrations; the maximum adsorption capacity was estimated to be 20.75 mg/g at 30 °C. The kinetic study also revealed that the adsorption process followed a pseudo-second-order model, with small RMSE and SAE values. FTIR and EXAFS analyses indicated that the Fe was chelated by $–NH_2$ and –OH groups on the CTS, and fluoride removal by Fe-CTS was due to Fe–F chelation, which occurred via ion exchange. These results suggest that Fe-CTS can be used as an effective adsorbent for fluoride removal.

Acknowledgements

This work was supported by National Natural Science Foundation of China (NSFC) (No. 21407129). This work also was supported by Beijing National Science Foundation (8144053). The authors want to thank the staff at the XAFS station (1W2B beamline) of the Beijing Synchrotron Radiation Facility for providing the beam time and assisting with the XAFS tests and data analysis.

References

[1] M. Sandip, T. Swagatika, P. Tapswani, K.S. Manoj, K.P. Raj, Removal efficiency of fluoride by novel Mg-Cr-Cl layered double hydroxide by batch process from water, Environ. Sci. 25 (2013) 993–1000.

[2] B. Krishna, G. Kaushik, G. Arijit, C.G. Uday, Fluoride removal efficiency from aqueous solution by synthetic iron(III)–aluminum(III)–chromium(III) ternary mixed oxide, Desalin. 255 (2010) 44–51.

[3] B. Kamel, P.K. Amid, Adsorption of fluoride onto crystalline titanium dioxide: Effect of pH, ionic strength, and co-existing ions, Colloid Interface Sci. 394 (2013) 419–427.

[4] WHO Repor. Fluoride and Fluorides: Environmental Health Criteria. World Health Organization, 1984.

[5] J.s. He, T. Siah, J.P. Chen, Performance of an optimized Zr-based nanoparticle-embedded PSF blend hollow fiber membrane in treatment of fluoride contaminated water, Water Res. 56 (2014) 88-97.

[6] W.X. Gong, J.H. Qu, R.P. Liu, H.C. Lan, Effect of aluminum fluoride complexation on fluoride removal by coagulation, Colloid Interface Sci. A: Physicochemical and Engineering Aspects. 395 (2012) 88– 93.

[7] S. Meenakshi, N. Viswanathan, Identification of selective ion-exchange resin for fluoride sorption, Colloid Interface Sci. 308 (2007) 438–450.

[8] P. Gwala, S. Andey, V. Mhaisalkar, P. Labhasetwar, S. Pimpalkar, C. Kshirsagar, Lab scale study on electrocoagulation defluoridation process optimization along with aluminium leaching in the process and comparison with full scale plant operation, Water Sci. Technol. 63 (2011) 2788-2795.

[9] I. Bejaoui, A. Mnif, B.Hamrouni, Influence of operating conditions on the retention of fluoride from water by nanofiltration, Desalin. and Water Treat. 29 (2011) 39–46.

[10] G. Moussavi, M. Mahmoudi, Degradation and biodegradability improvement of the reactive red 198 azo dye using catalytic ozonation with MgO nanocrystals, Chem. Eng. J. 152 (2009) 1–7.

[11] S. Raghu, C.W. Lee, S. Chellammal, S. Palanichamy, C.A. Basha, Evaluation of electrochemical oxidation techniques for degradation of dye effluents—A comparative approach, Hazard. Mater. 171(2009) 748–754.

[12] Q.J.Du, J.K. Sun, Y.H. Li, X.X. Yang, X.H. Wang, Z.H. Wang, L.H. Xia, Highly enhanced adsorption of congo red onto graphene oxide/chitosan fibers by wet-chemical etching off silica nanoparticles, Chem. Eng. J. 245 (2014) 99–106.

[13] S. Jagtap, M.K.N. Yenkie, N. Labhsetwar, S. Rayalu, Defluoridation of drinking water using chitosan based mesoporous alumina, Microporous and Mesoporous Mater. 142 (2011) 454–463.

[14] V. Tomar, S. Prasad, D. Kumar, Adsorptive removal of fluoride from aqueousmedia using Citrus limonum (lemon) leaf, Microchem. J. 112 (2014) 97–103.

[15] F. Ogata, H. Tominaga, H. Yabutani, N. Kawasaki, Removal of Fluoride ions from water by adsorption onto carbonaceous materials produced from coffee grounds, Oleo Sci. 60 (2011) 619-625.

[16] K. Gomoro, F. Zewge, B. Hundhammer, N. Megersa, Fluoride removal by adsorption on thermally treated lateritic soils, Chem. Soc. of Ethiop. 26 (2012) 361-372.

[17] W. Ma, F.Q. Ya, R. Wang, Y.Q. Zhao, Fluoride removal from drinking water by adsorption using bone char as a bioadsorbent, International J of Environ Technol and Manage. 9 (2008) 59-69.

[18] N. Chen, Z.Y. Zhang, C.P. Feng, M. Li, R.Z. Chen, N. Sugiura, Investigations on the batch and fixed-bed column performance of fluoride adsorption by Kanuma mud, Desalin. 268 (2011) 76–82.

[19] M. Barathi, A. Santhana Krishna Kumar, N. Rajesh, A novel ultrasonication method in the preparation of zirconium impregnated cellulose for effective fluoride adsorption, Ultrason. Sonochem. 21 (2014) 1090–1099.

[20] B.C. Pan, J.S. Xu, B. Wu, Z.G. Li, X.T. Liu, Enhanced Removal of Fluoride by Polystyrene Anion Exchanger Supported Hydrous Zirconium Oxide Nanoparticles, Environ. Sci. Technol. 47 (2013) 9347−9354.

[21] N. Chen, C.P. Feng, Z.Y. Zhang, R.P. Liu, Y. Gao, M. Li, N. Sugiura, Preparation and characterization of lanthanum(III) loaded granular ceramic for phosphorus adsorption from aqueous solution, Taiwan Inst. of Chem. Eng. 43 (2012) 783–789.

[22] S.Y. Zhang, Y. Lu, X.Y. Lin, X.S. Su, Y.L. Zhang, Removal of fluoride from groundwater by adsorption onto La(III)- Al(III) loaded scoria adsorbent, Appl. Surface Sci. 303 (2014) 1–5.

[23] X.L. Tang, H.Z. Zhang, S. Zhao, S.F. Gong, Removal of fluoride on chitosan coated alumina (CAL) from aqueous solution, Adv. Mater. Res. 518-523 (2012) 797-800.

[24] D. Thakre, S. Jagtap, N. Sakhare, N. Labhsetwar, S. Meshram, S. Rayalu, Chitosan based mesoporous Ti–Al binary metal oxide supported beads for defluoridation of water, Chem. Eng. J. 158 (2010) 315–324.

[25] J.J. García Sánchez, M. Solache Ríos, V. Martínez Miranda, C. Solís Morelos, Removal of fluoride ions from drinking water and fluoride solutions by aluminum modified iron oxides in a column system, Colloid Interface Sci. 407 (2013) 410–415.

[26] S. Meski, S. Ziani, H. Khireddine, S. Boudboub, S. Zaidi. Factorial design analysis for sorption of zinc on hydroxyapatite. Hazard. Mater. 2011, 186, 1007–1017.

[27] G. E. do Nascimento, M.M.M.B Duarte, N.F. Campos, C.M.B. de Menezes Barbosa, V.L. da Silva, Adsorption of the reactive gray BF-2R dye on orange peel: kinetics and equilibrium studies, Desalin. and Water Treat. 52 (2014) 1578–1588.

[28] F. Tümsek, O. Avcı, Investigation of kinetics and isotherm models for the acid orange 95 adsorption from aqueous solution onto natural minerals, Chemi & Eng Data. 58 (2013) 551−559.

[29] C. Sarici-ozdmir, Yunusonal, Error Anlaysis Studies of Dye Adsorption onto Activated Carbon from Aqueous Solutions, Part. Sci and Technol. 32 (2014) 20–27.

[30] A. Ghosh, K. Mukherjee, S.K. Ghosh, B. Saha, Sources and toxicity of fluoride in the environment,Res Chem Intermed. 39 (2013) 2881–2915.

[31] C.S. Shen, Y. Shen, Y.Z. Wena, H.Y. Wang, W.P. Liu, Fast and highly efficient removal of dyes under alkaline conditions using magnetic chitosan-Fe(III) hydrogel, water res. 45 (2011) 5200-5210.

[32] H.H. S, C.A. Demarchi, C.A. Rodrigues, J.M. Greneche, N. Nedelko, A.S. Waniewska, Adsorption of As(III) on chitosan-Fe-crosslinked complex (Ch-Fe), Chemosphere. 82 (2011) 278–283.

[33] N. Viswanathan, S. Meenakshi, Selective sorption of fluoride using Fe(III) loaded carboxylated chitosan beads, Fluor Chem. 129 (2008) 503–509.

[34] M.N. Sepehr, V. Sivasankar, M. Zarrabi, M.S. Kumar, Surface modification of pumice enhancing its fluoride adsorption capacity: An insight into kinetic and thermodynamic studies, Chem. Eng. J. 228 (2013) 192–204.

[35] H.Y. Zhu, R. Jiang, L. Xiao, G.M. Zeng, Preparation, characterization, adsorption kinetics and thermodynamics of novel magnetic chitosan enwrapping nanosized γ-Fe2O3 and multi-walled carbon nanotubes with enhanced adsorption properties for methyl orange, Bioresource Technol. 101 (2010) 5063–5069.

[36] Z.M. Ramirez, J.A.G. Calderon, A.A. Camarillo, J.C.F. Gonzalez, Adsorption and dehydrogenation of 2-propanol on the surface of γ-Al_2O_3-supported gold, Surface Sci. 606 (2012) 1167–1172.

[37] D. Thakre, S. Jagtap, N. Sakhare, N. Labhsetwar, S. Meshram, S. Rayalu, Chitosan based mesoporous Ti–Al binary metal oxide supported beads for defluoridation of water, Chem. Eng. J. 158 (2010) 315–324.

[38] R.B. Hernandez, A.P. Franco, O.R. Yola, A.L. Delgado, J. Felcman, M.A.L. Recio, A.L.R. Merce, Coordination study of chitosan and Fe^{3+}, Mol. Struct. 877 (2008) 89–99.

[39] L.H.V. Jimenez, R.H. Hurt, J. Matos, J.R.R. Mendez, Zirconium−Carbon Hybrid Sorbent for Removal of Fluoride from Water: Oxalic Acid Mediated Zr(IV) Assembly and Adsorption Mechanism, Environ. Sci. & Techno. 48 (2014) 1166−1174.

[40] L. Batistella, L.D. Venquiaruto, M.D. Luccio, J.V. Oliveira, S.B.C. Pergher, M.A. Mazutti, D. de Oliveira, A.J. Mossi, H. Treichel, R.Dallago, Evaluation of Acid Activation under the Adsorption Capacity of Double Layered Hydroxides of Mg-Al-CO_3 Type for Fluoride Removal from Aqueous Medium, Industrial & Eng Chem Res. 50 (2011) 6871–6876.

[41] M. Newville, IFEFFIT : interactive XAFS analysis and FEFF fitting, Synchrotron Radiat. 8 (2001) 322-324.

[42] B. Ravel, M. Newville, ATHENA, ARTEMIS, HEPHAESTUS: data analysis for X-ray absorption spectroscopy using IFEFFIT, Synchrotron Radiat. 12 (2005) 537-541.

[43] M.T. Klepka, N. Nedelko, J.M. Greneche, K. Lawniczak-Jablonska, I.N. Demchenko, A. Slawska-Waniewska, C.A. Rodrigues, A. Debrassi, C. Bordini, Local atomic structure and magnetic ordering of iron in Fe−chitosan complexes, Biomacromol. 9 (2008) 1586−1594.

[44] M. Santamaria, S. Terracina, Y. Konno, H. Habazaki, F.D. Quarto, Physicochemical characterization and photoelectrochemical analysis of iron oxide films, J. Solid State Electrochem. 17 (2013) 3005−3014.

[45] M.C. Smith, Y.M. Xiao, H.x. Wang, S.J. George, D. Coucouvanis, M. Koutmos, W. Sturhahn, et al. Normal-Mode Analysis of $FeCl_4$ - and $Fe_2S_2Cl_4$ 2- via Vibrational Mo1ssbauer, Resonance Raman, and FT-IR Spectroscopies, Inorg. Chem. 44 (2005) 5562-5570.

[46] Sanford A. Asher* and Todd M. Schuster, Differences in Iron-Fluoride Bonding between the Isolated Subunits of Human Methemoglobin Fluoride and Sperm Whale Metmyoglobin Fluoride As Measured by Resonance Raman Spectroscopyt, Biochemistry. 20 (1981) 1866-1873.

[47] N. Chen, Z.Y. Zhang, C.P. Feng, D.R. Zhu, Y.N. Yang, N. Sugiura, preparation and characterization of porous granular ceramic containing dispersed aluminum and iron oxides as adsorbents for fluoride removal from aqueous solution, Hazard. Mater. 186 (2011) 863–868.

[48] N. Chen, C.P. Feng, M. Li, Fluoride removal on Fe-Al-impregnated granular ceramic adsorbent from aqueous solution, Clean Techn Environ Policy. 16 (2014) 609–617.

[49] A. Tor, N. Danaoglu, G. Arslan, Y. Cengeloglu, Removal of fluoride from water by using granular red mud: Batch and column studies, Hazard. Mater. 164 (2009) 271–278.

[50] A. Ganapaty, V. Vellaisamy, R. Venkataraman, Fluoride sorption using cynodon dactylon-based activated carbon, Hem. ind. 65 (2011) 23-35.

[51] Y. Liu, J.T. Wang, Y.A. Zheng, A.Q. Wang, Adsorption of methylene blue by kapok fiber treated by sodium chlorite optimized with response surface methodology, Chem. Eng. J. 184 (2012) 248– 255.

[52] N. Özbay, A.F. YargJç, R.Z. Yarbay-Fahin, E. Önal, Full Factorial Experimental Design Analysis of Reactive Dye Removal by Carbon Adsorption, Chem. 1 (2013) 1-13.

[53] L.Y. Chai, Y.Y. Wang, N. Zhao, W.C. Yang, X.Y. You, Sulfate-doped Fe_3O_4/Al_2O_3 nanoparticles as a novel adsorbent for fluoride removal from drinking water, water res. 47 (2013) 4040-4049.

[54] S. Jagtap, M.K. Yenkie, S. Das, S. Rayalu, Synthesis and characterization of lanthanum impregnated chitosan flakes for fluoride removal in water, Desalin. 273 (2011) 267–275.

[55] Y. Yoon, J. Yoon, G. Amy, J. Chung, J. Sohn, Removal of toxic ions (chromate, arsenate, and perchlorate) using reverse osmosis, nanofiltration, and ultrafiltration menbranes, Chemosph. 77 (2009) 228-235.

[56] C.S. Shen, H. Chen, S.S. Wu, Y.Z. Wen, L.N. Li, Z. Jiang, M.C. Li, W.P. Liu, Highly efficient detoxification of Cr(VI) by chitosan–Fe(III) complex: Process and mechanism studies, Hazard. Mater. 244–245 (2013) 689–697.